

Article

# Comparative Effectiveness of Multiple Laser Scanning and Conventional Techniques on Zirconia Shear Bond Strength

Adil Othman Abdullah <sup>1</sup>, Yu Hui <sup>2</sup>, Sarah Pollington <sup>3</sup>, Fenik Kaml Muhammed <sup>1</sup>,  
Xudong Sun <sup>2</sup> and Yi Liu <sup>1,\*</sup>

<sup>1</sup> School of Stomatology, China Medical University, Shenyang 110002, China

<sup>2</sup> School of Environmental and Chemical Engineering, Dalian University, Dalian 116000, China

<sup>3</sup> Academic Unit of Restorative Dentistry, School of Clinical Dentistry, The University of Sheffield, Sheffield S10 2TA, UK

\* Correspondence: liuyi@cmu.edu.cn; Tel.: +86-24-3197-3999

Received: 3 April 2019; Accepted: 28 June 2019; Published: 2 July 2019



**Abstract:** This study aimed to compare the impact of different laser scanning with that of conventional methods on zirconia surface treatment through evaluation of shear bond strength (SBS) values. One hundred and thirty-two sintered zirconia cubic-samples were prepared and randomly divided into six study groups: milling control (without surface treatment); grinding; sandblasting; and three-times, four-times, and five-times laser scanning groups. The treatment process for the first three groups was performed before the zirconia coating, while the last three groups were treated after zirconia coating with veneer slurry through a spraying technique. In the current study, the surface roughness  $R_a$ , contact angle measurement, phase transformation, topography and interfaces, SBS in unaged and aged conditions, and fracture mode patterns of zirconia cores were investigated. The results were analyzed using laser confocal scanning microscopy, drop analyzer, X-ray diffractometry (XRD), scanning electron microscope (SEM) equipped with energy dispersive spectroscopy (EDS), universal testing machine and stereomicroscope. The results indicated that three-times laser scanned specimens presented higher  $R_a$  values than the other studied groups. The minimum contact angle value was detected in the mentioned group, while the control group presented the highest value. The XRD showed phase transformation from tetragonal to monoclinic t–m following grinding and sandblasting. However, the laser scanned specimens and the control group preserved the structural integrity of the zirconia core, presenting the tetragonal phase only. The highest SBS values were recorded in specimens treated with three-times laser scanning in the unaged and aged conditions. A mixed fracture was a common fracture pattern among the studied groups. The results confirmed that SBS could be optimized through three-times laser scanning and it provided better adhesion between zirconia and the veneer ceramic material. Multiple scanning processes of more than three times are not recommended for zirconia surface treatment.

**Keywords:** shear bond strength SBS; surface treatment; veneer ceramic; laser scanning; laser confocal microscopy

## 1. Introduction

The development of dental ceramics from their inception to modern ceramic compositions, along with different technologies, dates back to the 1770s [1]. Ceramics have become increasingly popular as restorative materials due to their inertness, aesthetics, and biocompatibility [1]. Ceramic materials have developed rapidly in the field of dentistry and have enabled the production of metal-free restorations, i.e., using all-ceramic materials [2].

Recently, the yttria-stabilized tetragonal zirconia polycrystal (Y-TZP) has become popular for the fabrication of all-ceramic crowns [3]. However, chipping is still a concern due to the relatively high failure rate among all-ceramic compared to metal–porcelain restorations [3].

Technological development in the dental industry, particularly in the field of ceramic materials, has enabled the production of all-ceramic materials due to a variety of highly sophisticated approaches [2]. Improvements in all-ceramic materials provide many advantages over the metal–porcelain system in terms of mechanical and physical properties [2].

Among ceramic materials, zirconia is one of the stable crystalline materials, with the crystalline content being zirconium oxide [4]. It provides satisfactory success rates, in comparison to the system of silica-based ceramics, in the load-bearing areas [5]. The color is similar to that of natural teeth and the mechanical properties are similar to those of metals [6]. The material is available in different forms such as tetragonal (t), cubic (c) and monoclinic (m) depending on the arrangement of the crystalline structure [7].

Certain variables play an essential role after surface treatment and improve the bond strength values between veneer/core materials [8]. Such variables include zirconia surface conditioning, internal stress resulting from the difference in the coefficient of thermal expansion, wetting property, and veneer ceramic shrinkage potential, which may influence the bonding strength of the veneer/core material [8].

Studies have investigated different techniques for treating zirconia core to optimize bond strength; these methods include grinding, sandblasting, laser scanning, airbrush spraying, and fine-brush painting approaches [9–12]. A five-year follow up survival rate of more than 90% was recorded by an *in vitro* study after surface modification following the sandblast technique [13]. However, some researchers have reported that grinding and sandblasting may lead to phase transformation from t–m resulting from shrinkage potential [14].

Conversely, it has been reported that combining  $ZrO_2$  with  $Y_2O_3$  preserves the material's mechanical behavior [15]. In the clinical oral environment, optimizing shear bond strength between the veneer/core material is an essential parameter to enable the longevity of all-ceramic fixed dental crowns FDCs when subjected to diverse occlusal and incisal forces [16].

A study has reported that enhancing the bond strength between the veneer/core is mandatory to yield the maximum fusion property between the two materials and secure a high success rate in fixed dental crowns [17]. There is no doubt that the potential problem that faces single or multi-unit FDCs is delamination or chipping of the veneer ceramic from its core. This may be due to the inadequate bond strength between the two materials [17].

Studies have reported delamination or chipping issues following surface treatment with zirconia as a common potential difficulty [18]. Five-year incidence rates of delamination issues in veneer ceramics were reported as 2.9% for metal–ceramic, while for zirconia the incidence rate was 2.8% [18]. However, another study has reported higher failure rates for zirconia crowns between 24–60 months follow-up [19].

The use of lasers in the dental field traces back to several decades ago when the impact of laser power on ceramic surfaces was investigated [20,21]. Currently, researchers are focusing on laser technology as a contemporary approach to optimize the surface properties of ceramic materials [22]. The most common types of laser that have been applied in the field include; Er:YAG, Nd:YAG, and  $CO_2$  laser [22]. Previous literature has reported that ceramic materials have the ability to absorb wavelengths sufficiently to permit laser treatment; therefore, the  $CO_2$  laser is recommended as an acceptable method for such surface treatment [23].

However, the application of laser scanning for zirconia coating has not been studied sufficiently. In this study, different laser scanning processes (L3, L4, and L5) were proposed for coating the zirconia core with a veneer ceramic (Noritake Cerabien ZR) material. These were compared to conventional methods, namely; grinding, sandblasting, and milling as a control group. Herein, different repeated laser scanning methods were undertaken to optimize the overall bonding strength of the veneer/core materials. The purposes of this study, therefore, were to evaluate the impact of different laser scanning processes on zirconia shear bond strength to veneering ceramic material and to compare

the effectiveness of the formerly mentioned scanning approaches with that of conventional methods. The hypothesis tested was that the shear bond strength between the veneer/core materials would not be superior in the laser scanning groups in comparison to that of the other conventional techniques.

## 2. Materials and Methods

### 2.1. Material Composition

The main components of veneer/core materials are summarized in Table 1.

**Table 1.** The ceramic materials used in the current study.

Materials	Type of Materials	Chemical Composition	Manufacturer Name
Zenostar®T	Y-TZP; Translucent, Yttria tetragonal zirconia polycrystal, the ceramic core material	ZrO <sub>2</sub> , HfO <sub>2</sub> , Y <sub>2</sub> O <sub>3</sub> , Y <sub>2</sub> O <sub>2</sub> , Aluminum oxide, and other oxides	Wieland Dental + Technik GmbH & Co. KG, Pforzheim, Germany
Noritake Cerabien ZR	Feldspar veneer ceramic	SiO <sub>2</sub> , Al <sub>2</sub> O <sub>3</sub> , Na <sub>2</sub> O, CaO, K <sub>2</sub> O, MgO, LiO <sub>2</sub> , B <sub>2</sub> O <sub>3</sub> , and pigments	Noritake Dental Supply Co., Osaka, Japan

### 2.2. Preparation of Zirconia Specimens

One hundred and thirty-two Zenostar®T Y-TZP (Wieland Dental + Technik GmbH & Co. KG, Pforzheim, Germany) cubic specimens were prepared by milling through computer aided design/computer aided manufacturing (CAD/CAM) machine (imes-icore GmbH, Eiterfeld, Germany). The specimens were sintered using a furnace machine (Austromat®, GmbH, Freilassing, Germany); the sintering protocol for a single crown is presented in Table 2.

**Table 2.** The sintering protocol for Zenostar®Translucent, applicable for a single crown prosthesis.

Condition	Temp <sup>1</sup> [°C]*	Temp <sup>2</sup> [°C]*	Heating Rate [°C/h]	Holding Time [h]
Heating	20	1520	1500	–
Constant temperature	1520	1520	–	0.5
Cooling	1520	300	800	–

\* Temp<sup>1</sup> and Temp<sup>2</sup> stand for starting the heat process with a low temperature and ending with a high temperature, respectively.

To achieve adequate dimensions of 10 mm × 10 mm for each zirconia core, a blue wax was sprayed, scanned, and designed to mill the required size of specimens. During the design of the cubic shape, the CAD/CAM software (SUM3D software v.7.1) automatically enlarged the specimens' dimensions to 11.2379 mm × 11.2379 mm (1.2379 mm added to the original required dimension) prior to performing the milling process. The achieved final dimensions were 10 mm × 10 mm after the sintering process. The amount of linear shrinkage was 11.02%. The surface of specimens was polished using the Zenostar®T polishing set. Specimens were cleaned ultrasonically in an ethanol solution used a digital ultrasonic cleaner for 10 min, then dried in a heat blast oven for 5 min at 90 °C before coating the specimens. Specimens were divided into the corresponding groups, as summarized in Table 3.

**Table 3.** Classification and description of experimental groups.

Groups	N	Description of Experimental Groups
Milling 'M'	22	The surface of specimens was not subjected to surface treatment, it was left as milled.
Grinding 'G'	22	The surface of the specimens was subjected to grinding.
Sandblasting 'S'	22	The surface of the specimens was subjected to sandblasting.
Three times, X3, laser scanning 'L3'	22	The surface of specimens was subjected to laser scanning for three times, after each scanning process the specimen was rotated 90°, then a new process was performed.
Four times, X4, laser scanning 'L4'	22	The surface of specimens was subjected to laser scanning for four times, after each scanning process the specimen was rotated 90°, then a new process was performed.
Five times, X5, laser scanning 'L5'	22	The surface of specimens was subjected to laser scanning for five times, after each scanning process the specimen was rotated 90°, then a new process was performed.

The density of zirconia specimens of the current study was measured following Archimedes' Principle:

$$\rho = \frac{m_1}{m_2 - m_3} \quad (1)$$

where  $\rho$ ,  $m_1$ ,  $m_2$  and  $m_3$  represent density, dry weight, wet weight, and floating weight, respectively. The density ( $\rho$ ) of zirconia after calculation was 6.016 g/cm<sup>3</sup>. The theoretical ( $\rho_{th}$ ), and relative densities ( $\rho_{rl}$ ) of zirconia core were also calculated according to the following equations:

$$\rho_{th} = \frac{m_{total}}{\frac{m_1}{\rho_1} + \frac{m_2}{\rho_2}} \quad (2)$$

where  $m_{total}$ ,  $m_1$ ,  $\rho_1$ ,  $m_2$ , and  $\rho_2$  refer to total mass; weight percent of the first phase, density of the first phase, weight percent of the second phase; and density of the second phase, respectively. From the XRD data, the weight percent and densities of the tetragonal and monoclinic phases were achieved and calculated. From the second equation, the theoretical density of zirconia was 6.024 g/cm<sup>3</sup>. The following equation was followed to calculate the relative density  $\rho_{rl}$ :

$$\rho_{rl} = \rho / \rho_{th} \times 100. \quad (3)$$

From the first two Equations (1) and (2), the values of density and theoretical density of the core material were achieved. The substitution of the recorded values in the third equation yielded the relative density  $\rho_{rl}$  (final density of zirconia); 99%.

### 2.3. Surface Treatment of Specimens Based on Assigned Groups

The surface treatment of the specimens ( $n = 132$ ) was followed using the techniques described in the present study. For the first control group (milling), the specimens ( $n = 22$ ) which were milled did not receive any surface treatment and were considered as a control group 'milling'. For group G, the specimens ( $n = 22$ ) were ground under wet conditions. A dental laboratory micromotor engine with a rotation of 35,000 rpm and a medium grit ceramic bur was used. A gentle motion from right to left was applied for 60 s on the targeted zirconia surface during the grinding process to minimize heat generation.

For the sandblasting, the specimens were subjected to 3.5 pressure bar for 10 s at a working distance of 15 mm used 125  $\mu$ m alumina particles (Refo, Qianshan, China). The direction of the air abrasion process was perpendicular to the specimen surface.

For the laser scanning groups, the core specimens were subjected to different scanning in terms of the number of times the scanning process was repeated. For the L3 group, the specimens were scanned three times. After the first scanning process, the specimens were rotated 90° and a second and then

third scanning process was carried out. The time interval between each rotation and starting a new scanning process was 5 s. For the L4 and L5 groups, a similar procedure was followed as described for the L3 group. For the laser scanning process, a CO<sub>2</sub> laser (JL-K6040, Julong Co.,Ltd, Shandong, China) was utilized. The laser parameters and properties are presented in Table 4.

**Table 4.** Laser (CO<sub>2</sub> laser) scanning parameters and properties.

Laser Parameters	Value	Laser Properties	Value
Scanning speed	30 mm·s <sup>-1</sup>	Wavelength	10.6 μm
Output power	25 W	Frequency	50 Hz
Distance between laser nozzle and zirconia	20 mm	Laser tube diameter	8 mm
Space between scanned lines	0.25 mm	Spot size	0.2 mm
Scanning duration	70 s	Intensity	0–1.6 × 10 <sup>6</sup> W/cm <sup>2</sup>
–	–	Pulse length	10–50 μs
–	–	Pulse energy	150 W
–	–	Feed speed	0–300 mm·s <sup>-1</sup>

For the first three groups, milling, grinding, and sandblasting (M, G, and S, respectively), the specimens' surface, based on their assigned groups, was coated with Noritake Cerabien ZR ( $n = 22$ , each group) veneer ceramic v–c materials (Noritake Dental Supply Co., Ltd, Nagoya, Japan) through airbrush spraying. Prior to performing the scanning process, the specimens' surface was coated with a thin film of v–c using the spraying method, followed by laser scanning. The experimental route is presented in Figure 1.

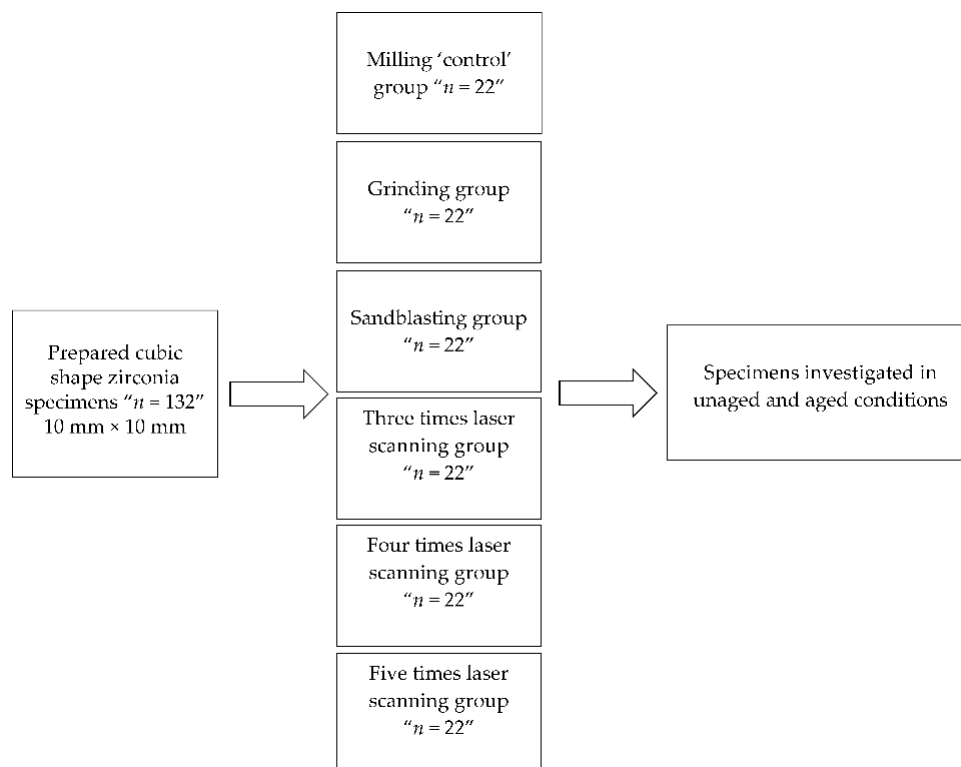


**Figure 1.** Flow chart summarizing the main experimental route.

#### 2.4. Airbrush Spraying Technique

To standardize the coating process, specimens were subjected to airbrush spraying to achieve a uniform film coating layer of v–c on the zirconia. The cubic zirconia specimen surface 10 mm × 10 mm was coated with Noritake Cerabien ZR (Noritake Dental Supply Co., Ltd, Nagoya, Japan). A digital analytical balance was utilized to weigh the veneer ceramic powder (Sartorius, Göttingen, Germany),

and the powder was then mixed with distilled water. To achieve a uniform mixture of v-c slurry, a mini magnetic stirrer was used at normal room temperature. To enable a uniform spraying process, specimens were positioned on a flat surface, and the distance between the zirconia and the laser nozzle tip was standardized at a fixed perpendicular distance of 15 cm. The coating protocol parameters, and airbrush spraying are summarized in Table 5.

**Table 5.** Coating parameters for airbrush spraying technique.

Coating Parameters	Values
Mixing of v-c powder with distilled water	1:1.5 ratio
Mixing speed and duration	300 *rpm/min for 10 min
Distance between zirconia and airbrush nozzle tip	15 cm
Nozzle diameter	0.2 mm
Working pressure	3.5 bar
Spray time	10 s
Dryness	4 min

\*rpm: rotations per minute.

To conduct laser scanning, specimens were transferred to the X-Y laser table and subjected to laser scanning of the air-sprayed surface area and complete coating with v-c material. After completing the process, specimens were left to cool down slowly at normal room temperature.

### 2.5. Analysis of Surface Roughness

Specimens were observed with a Confocal Laser Microscopy (CLM, LEXT 3D measuring laser microscope OLS40-SU, Olympus, Tokyo, Japan), followed by image processing through computer OLS4000 software (v.2.2.4) to achieve topographic images taken at different levels increasing in depth. The CLM image analysis of surface roughness was observed with the low-pass filter to assess color-graded fluorescence intensity. The images of the assigned core material specimens' surface were achieved by drawing three different line readings on the top surface of each specimen, and the mean values were calculated. The roughness values were performed for half of the specimens in each group based on the random selection of specimens.

### 2.6. Contact Angle Measurement

Contact angle values of specimens ( $n = 10$  in each group) were recorded. The sessile drop method (DataPhysics Instruments GmbH, Regensburg, Germany) software v.5.0.17 build 5017 was utilized to measure the contact angles. The solid-liquid angle was measured to assess the hydrophilic properties of the specimen surface. A time frame of 20 s was used to record the angle. The right and left angles were recorded for each droplet. Contact angles were achieved in a normal laboratory environment, and surface photographs were taken after droplets impacted on the core material in a stable and measurable state. The dosing volume of drop water was 3  $\mu\text{L}$ , and the dosing rate was 0.50  $\mu\text{L/s}$ . The procedure was repeated by the same trained operator.

### 2.7. X-Ray Diffractometry Examination

Phase transformation was detected through a SmartLab X-ray diffractometer (Rigaku, Tokyo, Japan) with Cu  $K\alpha$  radiation ( $\lambda$ ) of 1.5406 Å, at 200 mA and 40 kV. Diffraction data were collected within the  $2\theta$  range  $20^\circ$ – $90^\circ$  at a step size of  $0.02^\circ$  and a step time of 8 min. The peaks were read using the MDI Jade v6.0 software program to detect phases. The pattern of peaks was drawn using the OriginLab 2016 software (v.93E) program. The line positions at  $2\theta$  ( $^\circ$ ) were plotted against intensity (arbitrary units).

### 2.8. Scanning Electron Microscopy and Energy Dispersive Spectroscopy Examination

The zirconia specimens were randomly selected in each group ( $n = 1$  interface,  $n = 1$  top surface) and studied through SEM (ZEISS, Baden-Württemberg, Germany) equipped with EDS. The specimens were investigated for topography and interface. Specimens were sliced from the mid-part top to bottom to perform interface examination; the process was carried out used a slow speed diamond saw machine (Sherline, Vista, CA, USA) under water coolant. After the process, the interface was polished with SiC grit sizes #600 and #800 on a flat surface under running water. The gold-sputtering was conducted for specimens using a sputter coater machine. Specimens were investigated under different magnifications. Spot and line EDS spectra were also recorded and interpreted.

### 2.9. Veneering Procedure

Specimens ( $n = 20$ ; 10 specimens for unaged and 10 specimens for aged condition) for each group were ultrasonically cleaned with ethanol solution for 10 min and then dried in an oven. A silicon mold was used as a standard guide for preparing the veneer ceramic cylindrical shape Figure 2a. A recommended powder:liquid ratio was mixed to achieve a slurry mixture following manufacturer directions. The v-c slurry mixture was poured into the silicon mold (5 mm in diameter, 3 mm in height) through a hole to fabricate a cylindrically shaped v-c on zirconia core. The adhesion between the custom-made silicon mold and the veneer ceramic slurry was overcome through the application of a lubricating agent around a pre-made hole on the silicon mold.

Excess water from the slurry was controlled using tissue paper. The sintering procedure was conducted using a furnace machine Programat300 (Ivoclar Vivadent, Schaan, Liechtenstein, Germany) as presented in Table 6. To compensate the shrinkage potential of the v-c cylinder after the first firing cycle, a second layer was added, then fired.

**Table 6.** Sintering schedule of veneer ceramic material.

Veneer Ceramic	Pre-Drying			Firing Temperature (°C)	Holding Time (min)
	Temperature (°C)	Time (min)	Heating Rate (°C/min)		
Noritake Cerabien ZR	600	5	45	930	1

### 2.10. Shear Bond Strength Test Procedure

Specimens ( $n = 20$ ) were divided into unaged ( $n = 10$ ) and aged ( $n = 10$ ) conditions based on assigned groups, and the specimens in the latter group were preserved in distilled water. For conducting the shear bond strength test, specimens were positioned under the jig of a universal testing machine (MTS, Shenzhen, China) using a metal holder. The load was applied close to the interface between the veneer ceramic and the zirconia at a crosshead speed of 1 mm/min until failure of specimens was recorded (Figure 2b–d). The measured forces were recorded in MPa.

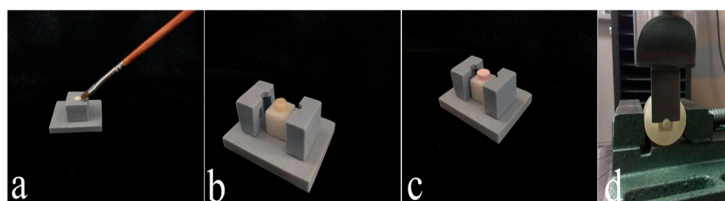


**Figure 2.** Illustration of the fabricated v-c cylinder and using the universal testing machine. The core material placed within the pre-fabricated silicon mold (a); the core placed outside the mold, the cylindrical shape of the v-c was set as 5 mm in diameter and 3 mm in height (b); fabricated v-c cylinder after firing cycles (c); a specimen placed under universal testing machine (d).

### 2.11. Fracture Mode Examination

To examine the type of fracture mode patterns, specimens were examined visually and through a stereomicroscope (RZ Series Zoom Stereo Microscope, MEIJI Techno, Saitama, Japan). The fracture mode patterns were classified as adhesive, cohesive, and “combination; mixed” types, respectively. The terms for each fracture category stand for separation of the veneer/core material from each other, separation through the veneer ceramic material, and a combination of the two previous modes “adhesive” and “cohesive” types, respectively. The fracture mode patterns were recorded for each assigned group.

### 2.12. Statistical Analysis

The results were statistically analyzed using SPSS software (v.20.0). The Kolmogorov–Smirnov normality test was applied for checking the distribution of surface roughness, contact angle, and shear bond strength values. The Levene statistic test was used to test the equality of the variances of the investigated groups. One-way ANOVA was used to compare means between groups for roughness, contact angle, and bond strength values. The ANOVA post hoc Tukey HSD test was performed for multiple comparisons of the mentioned groups.

To analyze the correlation ( $r$ ) between roughness and shear bond strength values, the Pearson correlation coefficient test was performed. The Pearson chi-square test was conducted for comparison of fracture mode patterns between studied groups. The univariate test was used to examine the impact of techniques, aging condition, and detect the impact of treatment on aging condition through tests of between-subjects effects while the shear bond strength was considered as a dependent variable. GraphPad Prism<sup>®</sup> Software (v.7.00) was used to create the graphs. The level of significance was set at  $\alpha = 0.05$ .

## 3. Results

The results for surface roughness, contact angle, and shear bond strength values are presented in Table 7. A statistically significant difference was observed between the studied groups in terms of surface roughness values for the M, S, and L3 groups ( $p < 0.05$ ). The L3 group provided the highest  $R_a$  value,  $1.1 \pm 0.23 \mu\text{m}$ , followed by the S group,  $1.02 \pm 0.17 \mu\text{m}$ . However, the control group, M, provided the lowest  $R_a$  value of  $0.72 \pm 0.2 \mu\text{m}$  in comparison to the other groups. The results were not statistically significant between groups M, G, L4 and L5 ( $p > 0.05$ ). Among the studied groups, a statistically significant difference was detected.

**Table 7.** Summarized results of surface roughness  $R_a$ , contact angle  $\theta$  measurement, and shear bond strength (SBS) values of studied groups.

Groups	$R_a$ Mean $\pm$ SD $\mu\text{m}$	$\theta$ Mean $\pm$ SD (deg.)	Unaged SBS Mean $\pm$ SD MPa	Aged SBS Mean $\pm$ SD MPa
Milling	$0.72 \pm 0.20^a$	$50.20 \pm 2.09^a$	$27.60 \pm 3.06^{a,c,d}$	$26.35 \pm 3.23^{a,b}$
Grinding	$0.97 \pm 0.25^{a,b}$	$48.70 \pm 2.21^a$	$27.44 \pm 4.04^{a,b,c,d}$	$26.19 \pm 3.39^{a,b}$
Sandblasting	$1.02 \pm 0.20^b$	$41.30 \pm 1.05^b$	$29.40 \pm 3.13^{a,b,d}$	$28.15 \pm 2.40^a$
L3	$1.10 \pm 0.23^b$	$37.30 \pm 1.33^d$	$31.70 \pm 2.90^a$	$29.80 \pm 2.97^a$
L4	$0.97 \pm 0.17^{a,b}$	$42.50 \pm 1.43^{b,c}$	$25.80 \pm 3.67^{c,d}$	$23.90 \pm 3.47^b$
L5	$0.95 \pm 0.21^{a,b}$	$44.40 \pm 1.95^c$	$24.40 \pm 4.27^c$	$22.50 \pm 3.06^b$

Values marked with superscript letters indicate statistically significant results between investigated groups ( $p < 0.05$ ).

Also, a statistically significant difference was observed for contact angle values among the studied groups ( $p < 0.05$ ). The highest value of the contact angle was recorded in group M,  $50.20^\circ \pm 2.09^\circ$ , while the lowest value was found in group L3,  $37.30^\circ \pm 1.33^\circ$ . A significant negative correlation was found between  $\theta$  and SBS values using the Pearson test ( $r = -0.5328$ ,  $R^2 = 0.2839$ ,  $p < 0.05$ ) as shown in Figure 3.

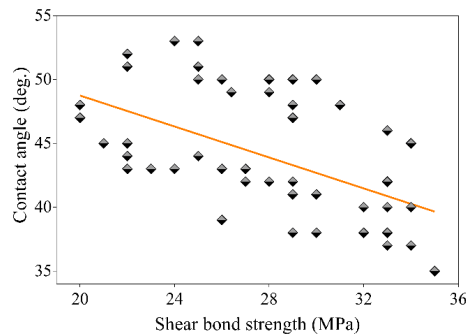


**Figure 3.** The plotted graph illustrates a statistically significant negative correlation ( $r$ ) between the contact angle and shear bond strength values ( $r = -0.5328$ ,  $p < 0.05$ ).

Specimens that showed low  $\theta$  yielded high shear bond strength (SBS) values. The measured contact angle for each group is demonstrated in (Figure 4a–f).

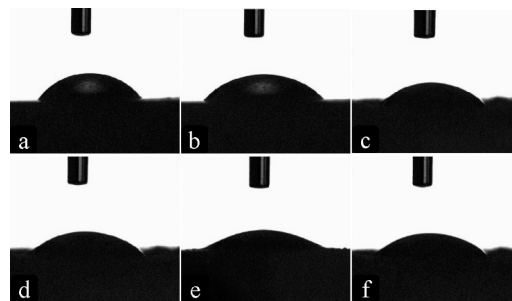


**Figure 4.** Illustrates sessile drop test, the contact angle was measured for specimens based on the assigned groups: milled (a); grinding (b); sandblasting (c); L3 (d); L4 (e); and L5 (f) groups, respectively.

The phase transformation was interpreted through XRD analyses, and phase transformations were not demonstrated following laser scanning processes or within the “control” milling group. Conversely, the grinding and sandblasting groups presented phase transformation from t–m (Figure 5a–e). The prominent peak of the tetragonal (t) phase was observed at  $2\theta$ :  $30.170^\circ$ ; corresponded to the crystallographic plane of XRD standard PDF#48-0224. The other (t) peaks were also found at  $2\theta$ :  $34.692^\circ$ ;  $35.115^\circ$ ;  $50.191^\circ$ ;  $50.503^\circ$ ;  $59.405^\circ$ ;  $59.967^\circ$ ;  $62.727^\circ$ ;  $73.202^\circ$ ;  $74.230^\circ$ ;  $81.662^\circ$  and  $82.151^\circ$ , respectively. The main monoclinic peak was found at  $2\theta$ :  $28.193^\circ$ ; corresponding to the crystallographic plane of XRD standard PDF#86-1449. The other monoclinic phases could also be found at  $24.062^\circ$ , and  $24.460^\circ$ , respectively.

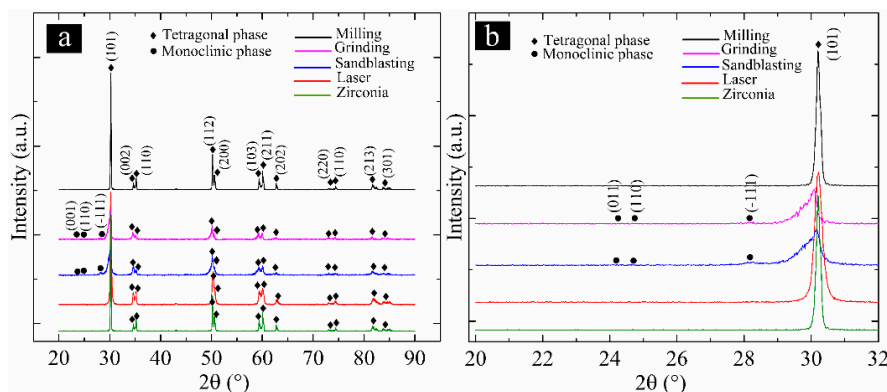


**Figure 5.** XRD showing crystallographic peaks; full scale (a) and enlarged scale (b). The core material shows different peaks following milling, grinding, sandblasting, laser scanning and zirconia without surface treatment.

The topography of specimens that were treated with laser scanning demonstrated obvious irregularities and displayed minimum micro-holes within the deposited v-c layer (Figure 6a–f). The “control” milling, grinding, and sandblasting techniques also presented irregularities, although fewer than in the laser treatment methods.

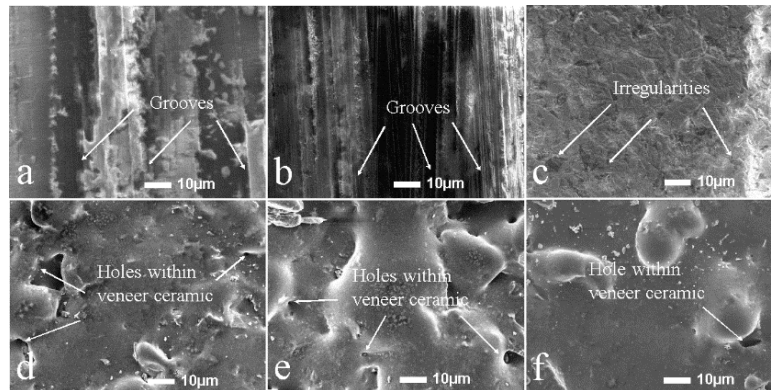


**Figure 6.** SEM (X500 magnifications) images show the topography of the core material following different techniques: milling (a); grinding (b); sandblasting (c); L3 (d); L4 (e) and L5 (f). The first three techniques were used to treat the core material before coating with v-c (a–c), the last three groups were subjected to a spraying technique in which zirconia was coated with v-c and laser scanned (d–f).

The laser scanning microscopy also confirmed topographical changes in 3D images after treatment of zirconia cores following conventional and laser mentioned techniques as shown in Figure 7a–f.

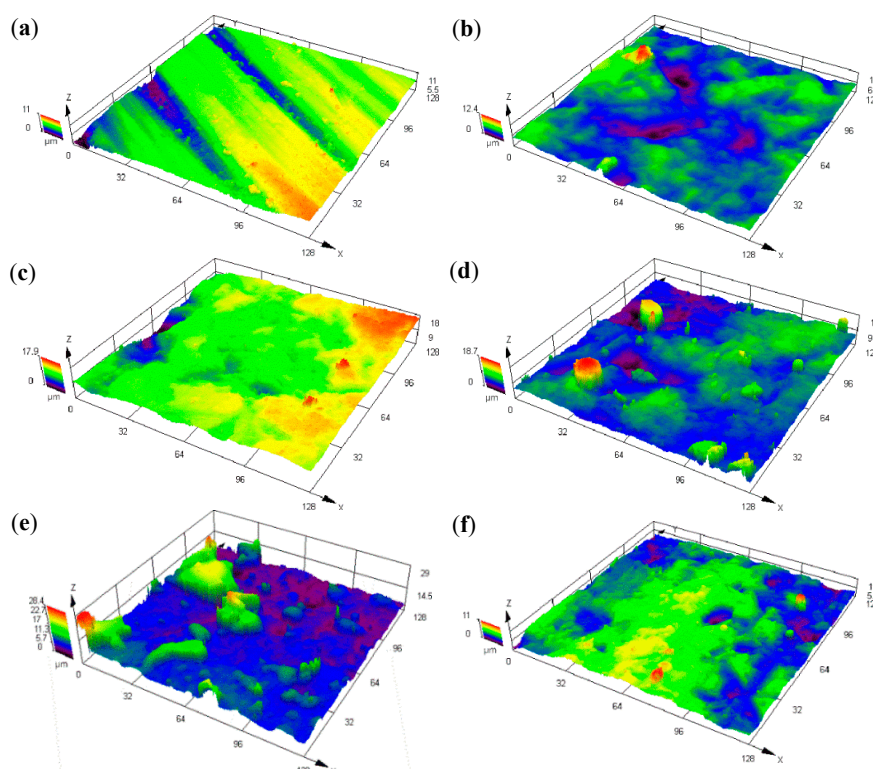


**Figure 7.** Laser confocal microscopy images demonstrating the topography of the treated core material following different techniques: milling (a); grinding (b); sandblasting (c); L3 (d); L4 (e) and L5 (f). The first three techniques were carried out prior to coating zirconia with v-c; the last three groups were coated with v-c using a spraying technique, and then the scanning process was performed.

Studied groups showed different interfaces following the various treatment techniques, as presented in Figure 8a–f. The interface areas between the veneer/core demonstrated certain irregularities, such as a few micro-gaps and tiny cracks following different treatment methods. A higher number of tiny cracks could be observed in the five-times laser scanning group than in the other groups. The interlocking property was detected between v–c and zirconia, in particular in the three- and four-times laser scanning specimens, where irregularities existed. However, conventional approaches including milling, grinding and sandblasting showed minimum interface irregularities in comparison to the laser processes.

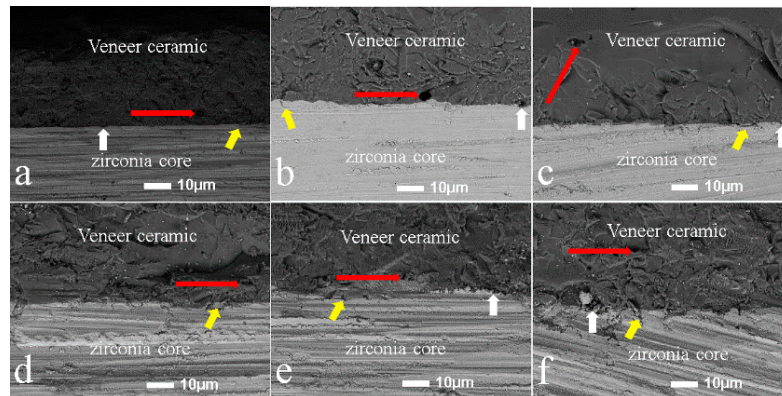


**Figure 8.** SEM (X500 magnifications) images illustrating different interfaces after coating zirconia with v–c material. The core material was treated by: milling (a); grinding (b); sandblasting (c); L3 (d); L4 (e) and L5 (f). The white arrows show adhesion between the veneer/core material; the yellow arrows show micro-cracks following different surface treatments; the red arrows show holes formed within the v–c layer which was deposited on the zirconia.

Results of the line EDS analyses are presented in Figure 9a–f. The results show that the test detected Si, Al, and Zr as the predominant components. Si and Al were found in the areas that were covered by the veneer ceramic material since these elements are the main component of the material, while Zr was observed in areas which were delaminated from the v–c material.

The results of SBS values following the mentioned techniques are presented in Table 7. The SBS values of specimens subjected to loading force in unaged condition showed a statistically significant difference between studied groups ( $p < 0.05$ ). The results showed that the highest mean of shear bond strength value was achieved in group L3;  $31.7 \pm 2.91$  MPa, while the lowest was in group L5;  $24.4 \pm 4.27$  MPa, followed by group L4;  $25.8 \pm 3.68$  MPa. The SBS values of specimens subjected to loading force in the aged condition showed a statistically significant difference between investigated groups ( $p < 0.05$ ). The results indicated that L5 group presented the lowest SBS value,  $22.5 \pm 3.06$  MPa; however, the highest was in L3 group;  $29.8 \pm 2.97$  MPa, followed by S group;  $28.15 \pm 2.4$  MPa. The Pearson test demonstrated a positive correlation between shear bond strength and roughness values ( $r = 0.7855$ ,  $R^2 = 0.617$ ,  $p < 0.05$ ) as shown in Figure 10.

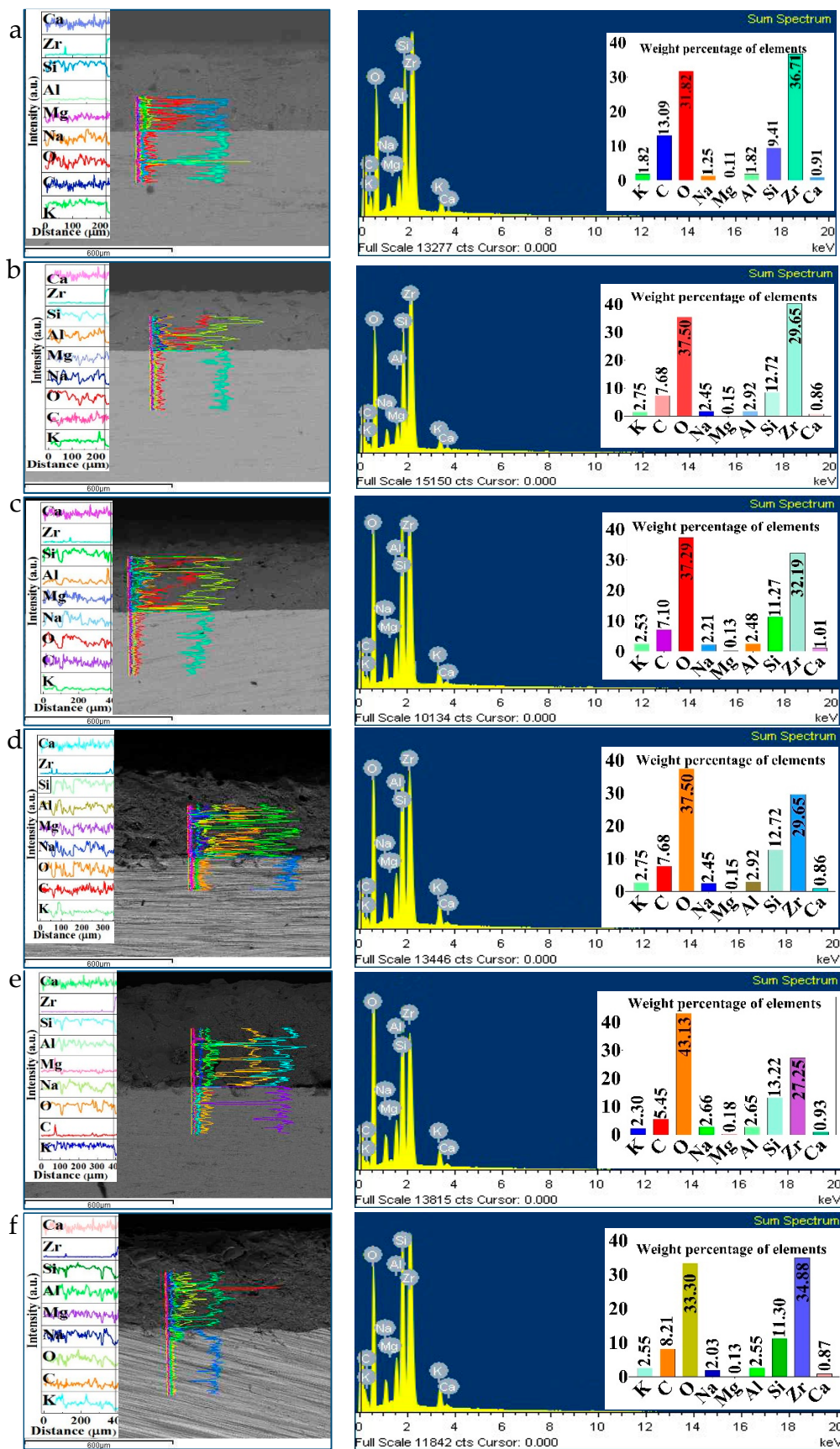
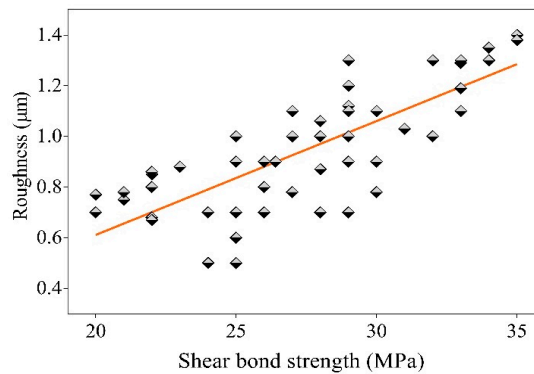


Figure 9. Line EDS analyses showing the elemental composition at the interfaces following different techniques: milling (a); grinding (b); sandblasting (c); L3 (d); L4 (e); and L5 (f), respectively.



**Figure 10.** Dot plot illustrating significant correlation ( $r$ ) between SBS and  $R_a$  values ( $r = +0.7855, p < 0.05$ ).

Sufficient bond strength values in specimens may have resulted from the existence of higher  $R_a$  values. The fracture mode patterns for the specimens in unaged and aged conditions are presented in Table 8.

**Table 8.** Summary of fracture mode patterns.

*Treatment Groups	Mode of Fracture (count)		
	Adhesive	Cohesive	Mixed
Milling	5	1	14
Grinding	2	1	17
Sandblasting	4	4	12
L3	2	6	12
L4	6	2	12
L5	6	2	12

\*The Pearson Chi-Square tests did not show a statistically significant difference in fracture mode patterns among investigated groups ( $p > 0.05$ ).

The highest number of the adhesive fracture mode were recorded in the M, L4, and L5 groups, respectively. However, the minimum value was observed in L3 group. The highest number of the cohesive fracture mode was detected among specimens in L3 group followed by the S group; the cohesive fracture mode was not detected in groups M and G, while this type of fracture pattern was the lowest in the L4 and L5 groups, respectively. The Pearson Chi-Square test did not show a statistically significant difference in fracture modes between the studied groups ( $p > 0.05$ ). The mixed fracture type is presented as a typical representation for fracture mode patterns that were observed for each of the investigated groups, as shown in Figure 11a–f.

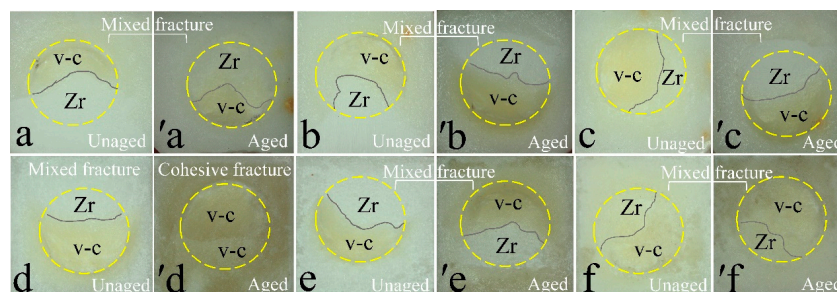


**Figure 11.** Fracture mode patterns shown under a stereomicroscope. The mixed fracture type was the common fracture among the studied groups in unaged and aged conditions: milling (a, a'), grinding (b, b') sandblasting (c, c'), L3 (d, d'), L4 (e, e'), and L5 (f, f) groups. The letters (a–f) and (a'–f') refer to unaged and aged conditions, respectively. The specimens in the “aged condition” were stored in distilled water for six weeks at 37 °C. The yellow circles show the border of the cylindrical veneer ceramics. The grey lines show the fracture lines.

The univariate general linear model was used to observe the impact of techniques and aging condition, also to observe the effect of treatment on aging condition via tests of between-subjects effects. The SBS was considered as a dependent variable, as shown in Table 9. The results demonstrated that treatment and aging condition presented statistically significant results ( $p < 0.05$ ), while the effect of treatment on aging condition was not shown the similar result ( $p > 0.05$ ).

**Table 9.** Tests of between-subject effects to show the influence of treatment techniques, aging condition, and the impact of treatment-aging; dependent variable is shear bond strength values.

Source	Type III Sum of Squares	df	Mean Square	F	Sig.
Corrected Model	766.553 <sup>a</sup>	11	69.687	6.245	0.000
Intercept	87064.694	1	87064.694	7801.865	0.000
Treatment	688.965	5	137.793	12.348	0.000
Aging	74.419	1	74.419	6.669	0.011
Treatment × aging	3.169	5	0.634	0.057	0.998
Error	1205.223	108	11.159	–	–
Total	89036.470	120	–	–	–
Corrected Total	1971.776	119	–	–	–

<sup>a</sup> R-squared = 0.389 (Adjusted R-squared = 0.327), Sig.: significant level.

#### 4. Discussion

Understanding the bonding strength between ceramics and corresponding veneer materials is an important area and needs to be studied sufficiently. The current study investigated different techniques for zirconia surface treatment to confirm which method could provide satisfactory results. Alternative zirconia surface treatments may optimize the mechanical properties between v–c and zirconia, including SBS, which plays an important role in extending the lifetime of fixed crowns in load-bearing areas [24]. Based on the results of the current study, the hypothesis of the experimental work which stated that the SBS between v–c and zirconia would not be superior via laser scanning compared to other techniques, was partially accepted. This is due to the fact that the L3 group provided better results than other groups; however, the L4 and L5 groups did not show superior results in comparison with the other techniques. In addition, the latter two techniques resulted in apparent color change, i.e., after exposing the core specimens to laser scanning process more than three times.

The current study found that the  $R_a$  was enhanced through repeating laser scanning, in particular L3, resulting in satisfactory SBS between the veneer/core material. A positive correlation was found between surface roughness and shear bond strength values, such that the rougher the surface, the higher were the SBS values. A study reported that different laser power might cause noticeable changes in the core material [25]. Previous literature has demonstrated that low output power has led to low surface damage compared with high power [25]. It is worth noting that low output power might not provide satisfactory roughness either [25]. Also, the variation in laser output power, in particular high power laser energy, enhanced the apparent bonding property [26]. The current study is consistent with the previous investigation in that the high laser output power yielded adequate  $R_a$  and resulted in sufficient SBS values [25].

The current study followed the sessile drop test to record contact angle  $\theta$  values between the liquid and solid surface [27]. High SBS values were correlated with the recorded low  $\theta$  due to the presence of different surface morphology in terms of roughness pattern; in particular, this was confirmed among L3 specimens which showed the minimum contact angle compared to the other groups. This finding is a suitable indicator to improve the surface wettability of zirconia when following the three-times laser scanning (L3), but this was not the case for other techniques. The result for L3 contradicted, but results for L4 and L5 agreed with, the previous investigation which claimed the minimum impact of CO<sub>2</sub> laser scanning on the contact angle [28]. It was apparent that the wetting property through L3 could be optimized.

XRD analysis showed that grinding and sandblasting led to a crystallographic change in zirconia from *t*-*m*, which is in agreement with previous studies [29,30]. However, the specimens that were treated by laser scanning, i.e., L3, L4 and L5, did not show phase transformation. The stability of zirconia following the laser scanning process, without presenting the monoclinic phase, is a positive indicator to preserve the structural integrity of zirconia.

Studies have reported different results following grinding and sandblasting techniques in terms of achieving optimum SBS values [24,31,32]. The current results show that the specimens that were treated with the laser scanning process, in particular L3, could better optimize bond strength than the other techniques without phase transformation. This may be attributed to the different methods which were used to treat core surfaces in the current study and in previous investigations.

The issue of flaw formation following the sandblast technique might lead to phase transformation [32], resulting from unequal stress distribution on the treated core surface and presenting an inferior mechanical property in the veneer/core material, resulting in delamination potential [33]. This may also adversely impact on the survival rate of fixed partial denture crowns in single and multiunit bridges [34]. The current study is consistent with previous studies in terms of the phase transformation from tetragonal to monoclinic [32].

Regarding the grinding technique, more inferior results than those for the sandblasting and L3 groups were observed. This may be due to the fact that the high heat generation during grinding of the core surface may lead to an adverse impact on the zirconia by causing phase transformation. The shear test recorded lower values than for the sandblast and L3 groups. Therefore, the property of bond strength might be detrimentally affected, and the grinding group specimens did not provide satisfactory results compared to the sandblast and L3 groups. This result is in agreement with previous studies [29,32,35].

It was observed that the top surface of the core material followed grinding and sandblasting showed different roughness properties [32,35]. The study also observed that the laser beam could result in certain micro-holes within the coated veneer ceramic material following the scanning process. These holes could play a role in micromechanical retention which improves the SBS between the veneer/core materials. The high output power which originated during laser scanning process may enhance such results. After conducting the SBS test, the surface of the core materials was subjected to certain internal pressure which led to the existence of micro-cracks at the interface. The repeated firing cycle may also play a pivotal role in the mentioned issue. After the SBS test, the surface of the core materials was subjected to certain internal pressure, which led to the existence of micro-cracks at the interface. The current results are consistent with the previously reported investigation [36]. In addition, the difference in irregularities between zirconia and veneer ceramic materials may be due to the methodology used in the current study. The laser scanning process created prominent irregularities in comparison to other methods; these results may be due to the laser power adsorption and repeated laser scanings.

It has been argued that mechanical and chemical bonding could play a significant role in the interface by providing sufficient adhesion property between the veneer/core materials [37]. EDS analyses detected different elemental compositions following coating of the core with the *v*-*c*. There was no significant elemental change after performing sintering or laser scanning. Also, the final density of the ceramic core presented the standard required value according to ISO 13356 [38].

Previous literature has found that on smooth core surfaces, the bond strength mostly depends on elements such as silica and oxygen and may act as a function of the surface chemistry and composition of zirconia, and not its surface texture [39]. The current study is in agreement with this literature since silica and oxygen were the predominant peaks on the flat zirconia core, which was covered by *v*-*c* material. Nevertheless, the specimens that presented a mixed type of fracture demonstrated zirconia in the delaminated area, while showing silica and oxygen as prominent peaks in the *v*-*c* areas. This might be attributed to the difference in the elemental compositions and microstructure of the *v*-*c* and zirconia core. The interlocking mechanism could also be increased through chemical bonding

and micromechanical interaction of the treated core material. The presence of high amounts of silica establishes the basis of chemical integration.

The fracture mode analysis presented different fracture patterns in the studied groups. In this study, the specimens in the L3 group showed the highest occurrence of the cohesive fracture type in comparison to other groups; the lowest value was recorded in the milling and grinding groups. The most predominant fracture type among specimens in the grinding group was the mixed fracture pattern. The highest numbers for the adhesive fracture type were observed in the L4 and L5 groups, respectively. In contrast, the grinding and L3 groups recorded the minimum number of the adhesive fracture type. It is believed that the cohesive fracture type might reflect acceptable SBS values between the veneer ceramic material and zirconia [40]. The existence of the cohesive fracture type as the highest number in the L3 group may be attributed to physical change, such as fusion between v-c and zirconia. The existence of the adhesive fracture mode among the milling, sandblasting, L4, and L5 groups might be due to inadequacy of the bond strength between v-c and zirconia. It was reported that the bond strength could be increased when the surface becomes rougher [41]. The Pearson test confirmed a positive correlation between surface roughness and the shear bond strength values. Thus, adequate treatment techniques and materials are critical to assist in achieving acceptable and durable veneer/core bonding.

The finding may be also due to mismatch of coefficient of thermal expansion (CTE) between the v-c and zirconia. A study has reported that a thermal mismatch of less than  $1 \times 10^{-6} \text{ K}^{-1}$  was considered acceptable since it did not lead to crack formation [42]. The materials used in this study have CTE values of  $9.1 \times 10^{-6} \text{ K}^{-1}$  and  $(10.5 \pm 0.5) \times 10^{-6} \text{ K}^{-1}$  for the veneer ceramic and the zirconia, respectively, based on the manufacturer's data. Further, the tests of between-subject effects when the shear bond strength was considered as a dependable variable, found that both treatment techniques and the aging condition should be taken into consideration during core surface treatment, since the results for both variables were significant ( $p < 0.05$ ). Therefore, accurate techniques should be applied to achieve satisfactory shear bond strength after surface treatment. In contrast, the impact of treatment on the aging condition was not statistically significant ( $p > 0.05$ ).

The L3 technique could be applied as a more recent approach than other techniques to treat the zirconia surface to protect it from chipping potential. The L3 scanning, which was simple to conduct, permitted the v-c material to be successfully deposited on the core material, provided enough roughness on the core material, and yielded satisfactory bond strength between veneer/core materials. This study demonstrated the reliability of the L3 technique and the suitability of the materials for implementation in a wide range of practical applications, in particular, fabricating fixed partial denture crowns including one or multiunit fixed bridges.

Regarding limitations of the current study, the present experimental work did not perform the following tests for the investigated groups: flexural strength test, 2-axis flexural strength, fatigue and fracture strength tests of the core material, CTE of the tested materials, and thermo-cycling testing. The impacts of scanning processes on the mechanical properties of ceramics, in particular, fatigue tolerance, three- and four-point flexural strength tests, and chemical composition changes could be further studied.

## 5. Conclusions

Within the limitations of the current study, the following conclusions can be drawn:

The three-times laser scanning proved to be the most reliable surface treatment method among the groups. Based on the current results, the study does not recommend multiple laser scanning for zirconia core material since repeating scanning processes four or five times was not more successful in providing better surface roughness and shear bond strength than other methods. Multiple laser scanning (i.e., four or five times) resulted in lowered shear bond strength and apparent color change on the core surface.

Grinding and sandblasting provided more satisfactory SBS values than the “milled” control group, and the four- and five-times laser scanning groups. The former two techniques showed phase transformation from t–m. The laser technique, in particular scanning three times, is a promising method to treat ceramic surface treatment without deterioration of structural integrity since it preserved elemental compositions and did not show phase transformation. The contact angle was proportionally related to the  $R_a$  and SBS values. The mixed fracture mode following laser scanning could be the most frequent fracture pattern. The laser scanning process provides better adhesion between, and a minimum gap between, the veneer/core materials at the interface, and limits hole formation within the v–c material. The incidence of micro-crack formation would be increased following multiple laser scanning.

**Author Contributions:** Conceptualization, A.O.A., S.P. and Y.L.; Data Curation, A.O.A., Y.H. and F.K.M.; Formal Analysis, A.O.A., Y.H., F.K.M. and Y.L.; Investigation, X.S.; Methodology, A.O.A., F.K.M. and Y.L.; Software, A.O.A., Y.H. and F.K.M.; Supervision, X.S. and Y.H.; Validation, A.O.A., X.S. and Y.H.; Visualization, X.S., S.P. and Y.L.; Writing—Original Draft, A.A.; Writing—Review and Editing, X.S., S.P. and Y.H.

**Funding:** This research was funded by Liaoning Province Natural Science, grant No. 20180550420, and Shenyang Science and Technology, grant No. 18-014-4-36.

**Acknowledgments:** The first author would like to express heartfelt gratitude to the Chinese Government Scholarship Council (CSC) for financial support throughout the study. The authors would also like to acknowledge Northeastern University, Institute of Metal Research, Chinese Academy of Sciences, and Qing Mei Dental Laboratory Technology Co., Ltd and Shenyangkede Aesthetic Studio Dental Laboratory in Shenyang, Liaoning Province, China for help provided during the experimental work.

**Conflicts of Interest:** The authors declare no conflicts of interest.

## References

- Zhang, Y.; Kelly, J.R. Dental ceramics for restoration and metal veneering. *Dent. Clin.* **2017**, *61*, 797–819. [[CrossRef](#)] [[PubMed](#)]
- Bajraktarova-Valjakova, E.; Korunoska-Stevkovska, V.; Kapusevska, B.; Gigovski, N.; Bajraktarova-Misevska, C.; Grozdanov, A. Contemporary dental ceramic materials, a review: Chemical composition, physical and mechanical properties, indications for use. *Open Access Maced. J. Med. Sci.* **2018**, *6*, 1742–1755. [[CrossRef](#)] [[PubMed](#)]
- Liu, D.; Matinlinna, J.P.; Tsoi, J.K.; Pow, E.H.; Miyazaki, T.; Shibata, Y.; Kan, C.W. A new modified laser pretreatment for porcelain zirconia bonding. *Dent. Mater.* **2013**, *29*, 559–565. [[CrossRef](#)] [[PubMed](#)]
- Eisenmenger-Sittner, C.; Nöbauer, C.; Mozetic, M.; Kovač, J.; Zaplotnik, R. Stabilization of tetragonal ZrO<sub>2</sub> by oxygen plasma treatment of sputtered ZrCu and ZrAl thin films. *Surf. Coat. Technol.* **2018**, *347*, 270–277. [[CrossRef](#)]
- Qeblawi, D.M.; Munoz, C.A.; Brewer, J.D.; Monaco, E.A., Jr. The effect of zirconia surface treatment on flexural strength and shear bond strength to a resin cement. *J. Prosthet. Dent.* **2010**, *103*, 210–220. [[CrossRef](#)]
- Manicone, P.F.; Iommetti, P.R.; Raffaelli, L. An overview of zirconia ceramics: Basic properties and clinical applications. *J. Dent.* **2007**, *35*, 819–826. [[CrossRef](#)] [[PubMed](#)]
- Shahmiri, R.; Standard, O.C.; Hart, J.N.; Sorrell, C.C. Optical properties of zirconia ceramics for esthetic dental restorations: A systematic review. *J. Prosthet. Dent.* **2018**, *119*, 36–46. [[CrossRef](#)]
- Her, S.B.; Kim, K.H.; Park, S.E.; Park, E.J. The effect of zirconia surface architecturing technique on the zirconia/veneer interfacial bond strength. *J. Adv. Prosthodont.* **2018**, *10*, 259–264. [[CrossRef](#)]
- Dapievie, K.S.; Guilardi, L.F.; Silvestri, T.; Rippe, M.P.; Pereira, G.K.R.; Valandro, L.F. Mechanical performance of Y-TZP monolithic ceramic after grinding and aging: Survival estimates and fatigue strength. *J. Mech. Behav. Biomed. Mater.* **2018**, *87*, 288–295. [[CrossRef](#)]
- Soltaninejad, F.; Valian, A.; Moezizadeh, M.; Khatiri, M.; Razaghi, H.; Nojehdehian, H. Nd:YAG laser treatment of bioglass-coated zirconia surface and its effect on bond strength and phase transformation. *J. Adhes. Dent.* **2018**, *20*, 379–387. [[CrossRef](#)]
- Muhammed, F.; Pollington, S.; Sun, X.; Abdullah, A.; Liu, Y. Novel coatings on zirconia for improved bonding with veneer ceramics. *Coatings* **2018**, *8*, 363. [[CrossRef](#)]

12. Caravaca, C.F.; Flamant, Q.; Anglada, M.; Gremillard, L.; Chevalier, J. Impact of sandblasting on the mechanical properties and aging resistance of alumina and zirconia based ceramics. *J. Eur. Ceram. Soc.* **2018**, *38*, 915–925. [[CrossRef](#)]
13. Sasse, M.; Kern, M. CAD/CAM single retainer zirconia-ceramic resin-bonded fixed dental prostheses: Clinical outcome after 5 years. *Int. J. Comput. Dent.* **2013**, *16*, 109–118. [[PubMed](#)]
14. Chevalier, J.; Gremillard, L.; Virkar, A.V.; Clarke, D.R. The tetragonal-monoclinic transformation in zirconia: lessons learned and future trends. *J. Am. Ceram. Soc.* **2009**, *92*, 1901–1920. [[CrossRef](#)]
15. Gautam, C.; Joyner, J.; Gautam, A.; Rao, J.; Vajtai, R. Zirconia based dental ceramics: structure, mechanical properties, biocompatibility and applications. *Dalton Trans.* **2016**, *45*, 19194–19215. [[CrossRef](#)]
16. Miyazaki, T.; Nakamura, T.; Matsumura, H.; Ban, S.; Kobayashi, T. Current status of zirconia restoration. *J. Prosthodont. Res.* **2013**, *57*, 236–261. [[CrossRef](#)]
17. Wang, G.; Zhang, S.; Bian, C.; Kong, H. Effect of zirconia surface treatment on zirconia/veneer interfacial toughness evaluated by fracture mechanics method. *J. Dent.* **2014**, *42*, 808–815. [[CrossRef](#)]
18. Pjetursson, B.E.; Valente, N.A.; Strasding, M.; Zwahlen, M.; Liu, S.; Sailer, I. A systematic review of the survival and complication rates of zirconia-ceramic and metal-ceramic single crowns. *Clin. Oral Implants Res.* **2018**, *29*, 199–214. [[CrossRef](#)]
19. Marefati, M.T.; Hadian, A.M.; Hooshmand, T.; Yekta, B.E.; Koohkan, R. Wettability of zirconia by feldspathic veneer in dental restorations: Effect of firing atmosphere and surface roughness. *Ceram. Int.* **2018**, *44*, 4307–4312. [[CrossRef](#)]
20. Yenisey, M.; Dede, D.Ö.; Rona, N. Effect of surface treatments on the bond strength between resin cement and differently sintered zirconium-oxide ceramics. *J. Prosthodont. Res.* **2016**, *60*, 36–46. [[CrossRef](#)]
21. Stubinger, S.; Homann, F.; Etter, C.; Miskiewicz, M.; Wieland, M.; Sader, R. Effect of Er:YAG, CO<sub>2</sub> and diode laser irradiation on surface properties of zirconia endosseous dental implants. *Lasers. Surg. Med.* **2008**, *40*, 223–228. [[CrossRef](#)] [[PubMed](#)]
22. Arami, S.; Tabatabae, M.H.; Namdar, S.F.; Chiniforush, N. Effects of different lasers and particle abrasion on surface characteristics of zirconia ceramics. *J. Dent. (Tehran)*. **2014**, *11*, 233–241.
23. Abdullah, A.O.; Hui, Y.; Sun, X.; Pollington, S.; Muhammed, F.K.; Liu, Y. Effects of different surface treatments on the shear bond strength of veneering ceramic materials to zirconia. *J. Adv. Prosthodont.* **2019**, *11*, 65–74. [[CrossRef](#)] [[PubMed](#)]
24. Kirmali, O.; Akin, H.; Ozdemir, A.K. Shear bond strength of veneering ceramic to zirconia core after different surface treatments. *Photomed. Laser Surg.* **2013**, *31*, 261–268. [[CrossRef](#)]
25. Ural, C.; KalyoncuoGlu, E.; Balkaya, V. The effect of different power outputs of carbon dioxide laser on bonding between zirconia ceramic surface and resin cement. *Acta. Odontol. Scand.* **2012**, *70*, 541–546. [[CrossRef](#)] [[PubMed](#)]
26. Abd El-Ghany, O.S.; Sherief, A.H. Zirconia based ceramics, some clinical and biological aspects: Review. *Future Dent. J.* **2016**, *2*, 55–64. [[CrossRef](#)]
27. Luo, F.; Hong, G.; Wang, T.; Jia, L.; Chen, J.Y.; Suo, L.; Pei, X.B.; Wan, Q.B. Static and dynamic evaluations of the wettability of commercial vinyl polysiloxane impression materials for artificial saliva. *Dent. Mater. J.* **2018**, *37*, 818–824. [[CrossRef](#)] [[PubMed](#)]
28. Chen, J.R.; Oka, K.; Kawano, T.; Goto, T.; Ichikawa, T. Carbon dioxide laser application enhances the effect of silane primer on the shear bond strength between porcelain and composite resin. *Dent. Mater. J.* **2010**, *29*, 731–737. [[CrossRef](#)]
29. Ryan, D.P.O.; Fais, L.M.G.; Antonio, S.G.; Hatanaka, G.R.; Candido, L.M.; Pinelli, L.A.P. Y-TZP zirconia regeneration firing: Microstructural and crystallographic changes after grinding. *Dent. Mater. J.* **2017**, *36*, 447–453. [[CrossRef](#)]
30. Tada, K.; Sato, T.; Yoshinari, M. Influence of surface treatment on bond strength of veneering ceramics fused to zirconia. *Dent. Mater. J.* **2012**, *31*, 287–296. [[CrossRef](#)]
31. Yamaguchi, H.; Ino, S.; Hamano, N.; Okada, S.; Teranaka, T. Examination of bond strength and mechanical properties of Y-TZP zirconia ceramics with different surface modifications. *Dent. Mater. J.* **2012**, *31*, 472–480. [[CrossRef](#)] [[PubMed](#)]
32. El-Shrkawy, Z.R.; El-Hosary, M.M.; Saleh, O.; Mona, M.H. Effect of different surface treatments on bond strength, surface and microscopic structure of zirconia ceramic. *Future Dent. J.* **2016**, *2*, 41–53. [[CrossRef](#)]

33. Kosmac, T.; Oblak, C.; Jevnikar, P.; Funduk, N.; Marion, L. Strength and reliability of surface treated Y-TZP dental ceramics. *J. Biomed. Mater. Res.* **2000**, *53*, 304–313. [[CrossRef](#)]
34. Monaco, C.; Tucci, A.; Esposito, L.; Scotti, R. Microstructural changes produced by abrading Y-TZP in presintered and sintered conditions. *J. Dent.* **2013**, *41*, 121–126. [[CrossRef](#)] [[PubMed](#)]
35. Khayat, W.; Chebib, N.; Finkelman, M.; Khayat, S.; Ali, A. Effect of grinding and polishing on roughness and strength of zirconia. *J. Prosthet. Dent.* **2018**, *119*, 626–631. [[CrossRef](#)]
36. Kim, J.W.; Covell, N.S.; Guess, P.C.; Rekow, E.D.; Zhang, Y. Concerns of hydrothermal degradation in CAD/CAM zirconia. *J. Dent. Res.* **2010**, *89*, 91–95. [[CrossRef](#)] [[PubMed](#)]
37. Inokoshi, M.; Yoshihara, K.; Nagaoka, N.; Nakanishi, M.; De Munck, J.; Minakuchi, S.; Vanmeensel, K.; Zhang, F.; Yoshida, Y.; Vleugels, J.; et al. Structural and chemical analysis of the zirconia-veneering ceramic interface. *J. Dent. Res.* **2016**, *95*, 102–109. [[CrossRef](#)]
38. *ISO 13356—Implants for Surgery—Ceramic Materials based on Yttria-Stabilized Tetragonal Zirconia (Y-TZP)*; ISO: Geneva, Switzerland, 2015.
39. Hooshmand, T.; Daw, R.; van Noort, R.; Short, R.D. XPS analysis of the surface of leucite-reinforced feldspathic ceramics. *Dent. Mater.* **2001**, *17*, 1–6. [[CrossRef](#)]
40. Fischer, J.; Grohmann, P.; Stawarczyk, B. Effect of zirconia surface treatments on the shear strength of zirconia/veneering ceramic composites. *Dent. Mater. J.* **2008**, *27*, 448–454. [[CrossRef](#)]
41. Abdullah, A.O.; Muhammed, F.K.; Yu, H.; Pollington, S.; Sun, X.; Liu, Y. The impact of laser scanning on zirconia coating and shear bond strength using veneer ceramic material. *Dent. Mater. J.* **2019**, *38*, 452–463. [[CrossRef](#)]
42. Steiner, P.J.; Kelly, J.R.; Giuseppetti, A.A. Compatibility of ceramic-ceramic systems for fixed prosthodontics. *Int. J. Prosthodont.* **1997**, *10*, 375–380. [[PubMed](#)]



© 2019 by the authors. Licensee MDPI, Basel, Switzerland. This article is an open access article distributed under the terms and conditions of the Creative Commons Attribution (CC BY) license (<http://creativecommons.org/licenses/by/4.0/>).